MIMO Radar Detection and Adaptive Design in Compound-Gaussian Clutter

Murat Akcakaya, *Student Member, IEEE* and Arye Nehorai*, *Fellow, IEEE*

Electrical and Systems Engineering Department.
Washington University in St.louis
St.louis, Missouri 63130
Emails: {makcak2, nehorai}@ese.wustl.edu

***Abstract*—Multiple-input multiple-output (MIMO) radars with widely separated transmitters and receivers are useful to discriminate a target from clutter using the spatial diversity of the scatterers in the illuminated scene. We consider the detection of targets in compound-Gaussian clutter. Compound-Gaussian clutter describes heavy-tailed distributions fitting high-resolution and/or low-grazing-angle radars in the presence of sea or foliage clutter. First, we introduce a data model using the inverse gamma distribution to represent the clutter texture. Then, we apply the parameter-expanded expectation-maximization (PX-EM) algorithm to estimate the clutter texture and speckle as well as the target parameters. We develop a statistical decision test using these estimates and approximate its statistical characteristics. Based on the approximation of the statistical characteristics of this test, we propose an algorithm to adaptively distribute the total transmitted energy among the transmitters. We demonstrate the advantages of MIMO and adaptive energy allocation using Monte Carlo simulations.**

I. Introduction

Multiple-input multiple-output (MIMO) radars with widely separated antennas exploit spatial diversity and hence the spatial properties of the targets' radar cross section (RCS). The RCSs of complex radar targets are quickly changing functions of the angle aspect. These target scintillations cause signal fading, which deteriorates the radar performance. When the transmitters are sufficiently separated, the multiple signals illuminate the target from de-correlated angles, and hence each signal carries independent information. This spatial diversity improves the radar performance by mitigating these scintillations. These systems have the ability to support high resolution target localization; improve the target parameter estimation and detection performance; and handle slow moving targets by exploiting Doppler estimates from multiple directions, see [1] and references therein.

We assume that the clutter reflections at the receiver follow the compound-Gaussian model. Target detection for MIMO systems has been addressed with white and colored Gaussian noise in [2] and [3], respectively. However, real clutter often deviates from the complex Gaussian model. Therefore, this conventional model cannot represent the heavy-tailed clutter statistics that are distinctive of several scenarios, e.g., high-resolution and/or low-grazing-angle radars in the presence of sea or foliage clutter [4], [5]. In our model, the compound-Gaussian clutter $\boldsymbol{e} = \sqrt{u}\mathcal{X}$, where u and $\mathcal{X}$ are the texture and speckle components of the compound model, respectively. The fast-changing $\mathcal{X}$ is a realization of a stationary zero mean complex Gaussian process, and the slow-changing u is modeled as a nonnegative real random process [6].

Clutter modeling with compound-Gaussian distribution requires selection of the texture characteristics. Gamma distribution for the texture is investigated in [7] for MIMO radar systems, leading to the well-known K clutter model. In this work, we specifically consider the inverse gamma distribution for texture component u, since similar to its gamma distributed counterpart inverse gamma fits well with real clutter data [8]. Moreover this choice of distribution results in a closed-form maximum likelihood solution for the joint target and clutter estimation [9].

The applications investigated for MIMO radar assume that the total energy is divided equally among the transmitters (see [1, Chapters 8 and 9]). We believe that this assumption may not be optimal, since MIMO radar systems are sensitive to RCS variations of the target w.r.t. angle and since transmitting signals with different energies from different transmitters may change the total received power under the same environmental conditions. Therefore, we extend our analysis in [10] and develop an adaptive algorithm that distributes the total energy among the transmitters, exploiting the RCS sensitivity of the system and optimizing detection performance.

The rest of the paper is organized as follows. In Section II, we introduce our parametric measurement model under the generalized multivariate analysis of variance (GMANOVA) framework [11] for the MIMO system. In Section III, we first present a parameter-expanded expectation-maximization (PX-EM) algorithm [12] with the use of the powerful GMANOVA tools to estimate the target and clutter parameters. Using these estimates, we then formulate a statistical decision test based on the generalized likelihood ratio (GLR) [13]. In Section IV, we develop the adaptive algorithm, and in Section V, we use Monte Carlo simulations to analyze the detection performance and improvements due to adaptive design. Finally we provide concluding remarks in Section VI.

This work was supported by the Department of Defense under the Air Force Office of Scientific Research MURI Grant FA9550-05-1-0443, and ONR Grant N000140810849.

978-1-4244-5813-4/10/$26.00 ©2010 IEEE

II. Radar Model

In this section, we develop measurement and statistical models for a MIMO radar system to detect a target in the range cell of interest (COI). Our goal is to present an algorithm, within a GMANOVA framework when the signal and noise parameters are unknown.

A. Measurement Model

We consider a two dimensional (2D) system with M transmitters and N receivers. Define $(x_{\mathrm{Tx}_m}, y_{\mathrm{Tx}_m})$, $m = 1, ..., M$, and $(x_{\mathrm{Rx}_n}, y_{\mathrm{Rx}_n})$, $n = 1, ..., N$, as the locations of the transmitters and receivers, respectively. We also assume a stationary point target located at (x_0, y_0) and having radar cross section (RCS) values changing w.r.to the angle aspect (e.g., multiple scatterers, which cannot be resolved by the transmitted signals, with (x_0, y_0) as the center of gravity) [1]. Define the complex envelope of the signal from the m^{th} transmitter is $\beta_m s_m(t)$, $m = 1, \ \ldots, \ M$, such that $|\beta_m|^2$ as the transmitted energy with $\sum_{m=1}^{M} |\beta_m|^2 = E$ (E is constant for any M) and $\int_{T_\mathrm{s}} |s_m(t)|^2 \mathrm{d}t = 1, \ m = 1, \ \ldots, \ M$, with T_s as the signal duration. We write the lowpass equivalent of the received signal at the n^{th} receiver following [1]:

$$r_n(t) = \sum_{m=1}^{M} \alpha_{nm}\sigma_{nm}\beta_m s_m(t - \tau_{nm})e^{-j\psi_{nm}} + e_n(t), \quad (1)$$

where

- σ_{nm} is the square root of the target RCS seen by the m^{th} transmitter and n^{th} receiver pair
- $\alpha_{nm} = \sqrt{\dfrac{G_{tx}G_{rx}\lambda^2}{(4\pi)^3 R_m^2 R_n^2}}$ is the channel parameter from the m^{th} transmitter to the n^{th} receiver, with G_{tx} and G_{rx} as the gains of the transmitting and receiving antennas, respectively; λ as the wavelength of the incoming signal; $R_m = \sqrt{(x_{\mathrm{Tx}_m} - x_0)^2 + (y_{\mathrm{Tx}_m} - y_0)^2}$ and $R_n = \sqrt{(x_{\mathrm{Rx}_n} - x_0)^2 + (y_{\mathrm{Rx}_n} - y_0)^2}$ as the distances from transmitter and receiver to target, respectively
- $\tau_{nm} = (R_m + R_n)/c$, and c is the speed of the signal propagation in the medium
- $\psi_{nm} = 2\pi f_\mathrm{c}\tau_{nm}$, with f_c as the carrier frequency
- $e(t)$ is additive clutter noise.

To enable the data separation at the receiver side arriving from the different transmitters, we assume low–cross-correlation transmitted signals. The design of signals with these properties is a challenging research subject [14], but for simplification of the problem and demonstration of our methods and analysis, we assume that the required signal criteria are met (this assumption is commonly made for MIMO radar, see [1, Chapters 8 and 9] and references therein.) Hence, we apply matched-filtering and obtain the output of the n^{th} receiver corresponding to the i^{th} transmitter :

$$r_{ni} = \beta_i\alpha_{ni}\sigma_{ni}e^{-j\psi_{ni}} + e_{ni}, \quad (2)$$

where $r_{ni} = \int_{\tau_{ni}}^{\tau_{ni}+T_\mathrm{s}} r_n(t)s_i^*(t - \tau_{ni})\mathrm{d}t$ and $e_{ni} = \int_{\tau_{ni}}^{\tau_{ni}+T_\mathrm{s}} e_n(t) \ s_i^*(t - \tau_{ni})\mathrm{d}t$.

Then, combining the received data corresponding to the transmitted signal $s_i(t)$ for one pulse, we obtain

$$\boldsymbol{r_i} = \boldsymbol{A}_i\boldsymbol{x}_i + \boldsymbol{e}_i, \quad (3)$$

where

- $\boldsymbol{r_i} = [r_{1i}, \ \ldots, \ r_{Ni}]^T$
- $\boldsymbol{A}_i = \beta_i\mathrm{diag}(\alpha_{1i}e^{-j\psi_{1i}}, \ \ldots, \ \alpha_{Ni}e^{-j\psi_{Ni}})$
- $\boldsymbol{x}_i = [\sigma_{1i}, \ \ldots, \ \sigma_{Ni}]^T$
- $\boldsymbol{e}_i = [e_{1i}, \ \ldots, \ e_{Ni}]^T$.

We stack the receiver outputs corresponding to all the signals into an $NM \times 1$ vector

$$\boldsymbol{y} = \boldsymbol{A}\boldsymbol{x} + \boldsymbol{e}, \quad (4)$$

where

- $\boldsymbol{y} = [\boldsymbol{r}_1^T, \ \ldots \ \boldsymbol{r}_M^T]^T$
- $\boldsymbol{A} = \mathrm{blkdiag}(\boldsymbol{A}_1, \ \ldots, \ \boldsymbol{A}_M)$
- $\boldsymbol{x} = [\boldsymbol{x}_1^T, \ \ldots \ \boldsymbol{x}_M^T]^T$
- $\boldsymbol{e} = [\boldsymbol{e}_1^T, \ \ldots \ \boldsymbol{e}_M^T]^T$.

We transmit K pulses and assume that the target is stationary during this observation time; then

$$\boldsymbol{Y} = [\boldsymbol{y}(1) \ \boldsymbol{y}(2) \ \cdots \ \boldsymbol{y}(K)]_{NM\times K} = \boldsymbol{A}\boldsymbol{x}\boldsymbol{\phi} + \boldsymbol{E}, \quad (5)$$

where $\boldsymbol{\phi} = [1, \ \ldots \ 1]_{1\times K}$, and $\boldsymbol{E} = [\boldsymbol{e}(1) \ \boldsymbol{e}(2) \ \cdots \ \boldsymbol{e}(K)]_{NM\times K}$ is the additive noise.

B. Statistical Model

In (5), we assume that $\boldsymbol{X}$ (target RCS values) is unknown deterministic.

We consider the compound-Gaussian distribution $\boldsymbol{e}(k)$=$\sqrt{u(k)}\mathcal{X}(k)$, $k = 1, \ \ldots, \ K$, to model the clutter with $u(k)$ and $\mathcal{X}(k)$ as the texture and speckle components, respectively; see [9] and references therein. The realizations of the fast-changing component, $\mathcal{X}(k)$, $k = 1, \ \ldots, \ K$, are independent and identically distributed (i.i.d.) and follow a complex Gaussian distribution with zero mean and covariance $\boldsymbol{\Sigma}$. The texture is the slow-changing component [6]; thus we consider it to be constant during the pulse duration T_s. However, we also assume the texture to be an independent realization of the same random process from pulse to pulse; *i.e.,* $\mathrm{Cov}(u(k), u(k^{'})) = 0$ for $k \neq k^{'}$. Therefore, $\boldsymbol{e}(k)$ $k = 1, ..., K$, are i.i.d., and we can write the conditional distribution for the observation $\boldsymbol{Y}$ in (4) as

$$\prod_{k=1}^{K} p_{\boldsymbol{y}|u}(\boldsymbol{y}(k)|u(k)) = \prod_{k=1}^{K} \frac{1}{|\pi u(k)\boldsymbol{\Sigma}|} \exp\Big\{-[\boldsymbol{y}(k) - \boldsymbol{A}\boldsymbol{x}\phi(k)]^H \cdot [u(k)\boldsymbol{\Sigma}]^{-1}[\boldsymbol{y}(k) - \boldsymbol{A}\boldsymbol{x}\phi(k)]\Big\}, \quad (6)$$

where"$(\cdot)^H$" denotes the Hermitian transpose.

Observe that (5) , conditioned on $u(k)$, $k = 1, \ \ldots, \ K$, with known $\boldsymbol{A}$ and $\boldsymbol{\phi}$ and unknown $\boldsymbol{x}$ and $\boldsymbol{\Sigma}$, is a GMANOVA model. We assume that $w(k) = 1/u(k)$ follows the gamma distribution (consequently $u(k)$ follows the inverse gamma distribution) with unit mean and unknown shape parameter $v > 0$ as in [9]; *i.e.,*

$$p_w(w(k); v) = \frac{1}{\Gamma(v)} v^v w(k)^{v-1} \exp\left[-vw(k)\right], \quad (7)$$

where $\Gamma(\cdot)$ is the gamma function. Therefore, we consider $\boldsymbol{x}$, $\boldsymbol{\Sigma}$, and v as the unknown parameters.

III. Detection and Estimation Algorithms

We present in this section the maximum likelihood estimation (MLE) of the unknown parameters and target detection test. We derive a statistical decision test based on GLR using the observed data likelihood function to determine the presence of a target in the COI. We choose between two hypotheses in the following parametric test:

$$\begin{cases} \mathcal{H}_0: & \boldsymbol{x}=\boldsymbol{0}, \boldsymbol{\Sigma}, v \\ \mathcal{H}_1: & \boldsymbol{x}\neq\boldsymbol{0}, \boldsymbol{\Sigma}, v \end{cases}, \tag{8}$$

with the speckle covariance $\boldsymbol{\Sigma}$ and the inverse texture shape parameter v as the nuisance parameters. We compute the GLR test by replacing the unknown parameters with their MLEs in the likelihood ratio test. Then, we reject $\mathcal{H}_0$ (target-free case) in favor of $\mathcal{H}_1$ (target-present case) when

$$\text{GLR} = \frac{p_1(Y;\hat{\boldsymbol{x}}_1,\hat{\boldsymbol{\Sigma}}_1,\hat{v}_1)}{p_0(Y;\hat{\boldsymbol{\Sigma}}_0,\hat{v}_0)} > \eta, \tag{9}$$

where $p_0(\cdot)$ and $p_1(\cdot)$ are the observed data likelihood functions under $\mathcal{H}_0$ and $\mathcal{H}_1$. Moreover, $\hat{\boldsymbol{\Sigma}}_0$ and $\hat{\boldsymbol{\Sigma}}_1$ are the MLEs of $\boldsymbol{\Sigma}$, and $\hat{v}_0$ and $\hat{v}_1$ are the MLEs of the shape parameter v under $\mathcal{H}_0$ and $\mathcal{H}_1$; $\hat{\boldsymbol{x}}_1$ is the MLE of $\boldsymbol{x}$ under $\mathcal{H}_1$; η is the detection threshold. For this special case of compound-Gaussian model with inverse gamma texture, it is easy to obtain a closed-form expression for the marginal pdf $p_{\boldsymbol{y}}(\cdot)$ of $\boldsymbol{y}(k)$, which is a complex multivariate t distribution [9].

We compute the MLEs of the vector $\boldsymbol{x}$, speckle covariance matrix $\boldsymbol{\Sigma}$, and texture distribution shape parameter v using the hierarchical data model presented in (6) and (7). We consider two iterative loops for the MLE computations: (i) inner loop and (ii) outer loop. In the inner loop, first we introduce the PX-EM algorithm to obtain the MLEs $\hat{\boldsymbol{x}}$ and $\hat{\boldsymbol{\Sigma}}$ for a fixed v. The PX-EM algorithm has the same convergence properties as the classical EM algorithm, but it outperforms the EM algorithm in global rate of convergence [12]. In the outer loop, we estimate v using the MLEs from the inner loop [9].

1) Inner Loop: PX-EM algorithm for inverse gamma texture.-

Recall that $\boldsymbol{x}$, $\boldsymbol{\Sigma}$, and v are the unknown parameters. We first estimate $\boldsymbol{\theta}=\{\boldsymbol{x},\boldsymbol{\Sigma}\}$, assuming that v is known. We implement the PX-EM algorithm by adding a new unknown parameter μ_w, the mean of $w(k)$, to this set; *i.e.*, $\boldsymbol{\theta_*}=\{\boldsymbol{x},\boldsymbol{\Sigma}_*,\mu_w\}$. In this model, since the maximization step performs a more efficient analysis by fitting the expanded parameter set, the PX-EM algorithm has a rate of convergence at least as fast as the EM algorithm [12]. Under this expanded model the pdf of $w(k)$ is

$$p_w(w(k);v,\mu_w) = \frac{1}{\Gamma(v)}\left(\frac{v}{\mu_w}\right)^v w(k)^{v-1}\exp\left[-vw(k)/\mu_w\right]. \tag{10}$$

Consider $\boldsymbol{\theta} = R(\boldsymbol{\theta_*}) = \{\boldsymbol{x},\boldsymbol{\Sigma}_*/\mu_w\}$, where $R(\cdot)$ is the reduction function (many-to-one) from the expanded to the original space. Moreover, $\mu_w^0=1$ is the null value such that the complete-data model is preserved.

Since the complete-data likelihood function belongs to an exponential family, we simplify the PX-EM algorithm following [15]. Thus the PX-E step reduces to calculating the conditional expectation of the natural complete-data sufficient statistics given the observed data and expanded unknown parameters with $\mu_w=\mu_w^0$. Then, the PX-M step simply replaces the natural complete-data sufficient statistics in the MLE expressions of $\boldsymbol{x}$, $\boldsymbol{\Sigma}_*$ and μ_w with their conditional expectations obtained in the PX-E step.

We find the expressions for the MLEs of $\boldsymbol{x}$, $\boldsymbol{\Sigma}_*$, and μ_w using the complete data log-likelihood function. These MLEs can be shown to be functions of the natural complete-data sufficient statistics. Since (5) is a GMANOVA model, we use the results of [11] for the MLEs of $\boldsymbol{x}$ and $\boldsymbol{\Sigma}_*$ and the results of [9, Appendix A] for the PX-EM algorithm.

We define i and j as the inner and outer loop iteration indexes, respectively. We summarize the algorithm:

PX-E Step: Calculate the conditional expectation of the sufficient statistics under $\mathcal{H}_1$, concentrated at $\hat{v}^{(j)}$, the j^{th} iteration step estimate of v

Using the properties of the compound-Gaussian model with inverse gamma distributed texture [16], we observe that $w(k)|y(k)$ follows a gamma distribution with

$$\begin{aligned} \hat{w}_1^{(i)}(k) &= \mathrm{E}_{w|y}[w(k)|\boldsymbol{y}(k);\hat{\boldsymbol{\theta}}_*^{(i)}] \\ &= (\hat{v}^{(j)}+MN)\cdot\left\{\hat{v}^{(j)}+d(k,\hat{\boldsymbol{\theta}}_*^{(i)})\right\}^{-1}, \end{aligned} \tag{11}$$

where $\hat{\boldsymbol{\theta}}_*^{(i)} = \{\hat{\boldsymbol{x}}^{(i)},\hat{\boldsymbol{\Sigma}}_*^{(i)},\hat{\mu}_w^{(i)}=\hat{\mu}_w^0=1\}$ is the estimate of $\boldsymbol{\theta}_*$ at the i^{th} iteration and $d(k,\hat{\boldsymbol{\theta}}_*^{(i)}) = \left[\boldsymbol{y}(k)-\boldsymbol{A}\hat{\boldsymbol{x}}^{(i)}\phi(k)\right]^H\left[\hat{\boldsymbol{\Sigma}}^{(i)}\right]^{-1}\left[\boldsymbol{y}(k)-\boldsymbol{A}\hat{\boldsymbol{x}}^{(i)}\phi(k)\right]$. Then,

$$T_1^{(i)} = \frac{1}{K}\sum_{k=1}^{K}\boldsymbol{y}(k)\phi(k)^H\hat{w}_1^{(i)}(k) \tag{12a}$$

$$T_2^{(i)} = \frac{1}{K}\sum_{k=1}^{K}\boldsymbol{y}(k)\boldsymbol{y}(k)^H\hat{w}_1^{(i)}(k) \tag{12b}$$

$$T_3^{(i)} = \frac{1}{K}\sum_{k=1}^{K}\phi(k)\phi(k)^H\hat{w}_1^{(i)}(k) \tag{12c}$$

$$T_4^{(i)} = \frac{1}{K}\sum_{k=1}^{K}\hat{w}_1^{(i)}(k) \tag{12d}$$

For the PX-M step, we first define $S^{(i)} = T_2^{(i)} - T_1^{(i)}\left(T_3^{(i)}\right)^{-1}\left(T_1^{(i)}\right)^H$ and $Q^{(i)} = \boldsymbol{A}\left[\boldsymbol{A}^H\left(S^{(i)}\right)^{-1}\boldsymbol{A}\right]^{-1}\boldsymbol{A}^H$.

PX-M Step:

$$\hat{\boldsymbol{x}}_1^{(i+1)} = \left[\boldsymbol{A}^H \left(S^{(i)}\right)^{-1} \boldsymbol{A}\right]^{-1} \boldsymbol{A}^H \cdot \left(S^{(i)}\right)^{-1} T_1^{(i)} \left(T_3^{(i)}\right)^{-1}, \quad (13a)$$

$$\hat{\boldsymbol{\Sigma}}_*^{(i+1)} = \left(S^{(i)}\right)^{-1} + \left[I_{MN} - Q^{(i)} \left(S^{(i)}\right)^{-1}\right] T_1^{(i)} \cdot \left(T_3^{(i)}\right)^{-1} \left(T_1^{(i)}\right)^H \cdot \left[I_{MN} - Q^{(i)} \left(S^{(i)}\right)^{-1}\right]^H, \quad (13b)$$

$$\hat{\mu}_w^{(i+1)} = T_4^{(i)}, \quad (13c)$$

$$\hat{\boldsymbol{\Sigma}}_1^{(i+1)} = \hat{\boldsymbol{\Sigma}}_*^{(i+1)} / \hat{\mu}_w^{(i+1)}, \quad (13d)$$

Under $\mathcal{H}_0$, we calculate $\hat{\boldsymbol{\Sigma}}_0$, with $\boldsymbol{x} = \boldsymbol{0}$, and update the sufficient statistics accordingly.

2) Outer Loop: MLE of the shape parameter of the inverse gamma texture.

We compute $\hat{v}^{(j+1)}$ by maximizing the concentrated observed data ($\boldsymbol{y}(k)$, $k = 1, \ldots, K$) log-likelihood function using the estimates from the PX-EM step. We denote $\hat{\boldsymbol{x}}^{(\infty)}$, $\hat{\boldsymbol{\Sigma}}_0^{(\infty)}$, and $\hat{\boldsymbol{\Sigma}}_1^{(\infty)}$ as the estimates of $\boldsymbol{x}$ and $\boldsymbol{\Sigma}$ obtained upon the convergence of the inner loop and compute

$$\hat{v}_1^{(j+1)} = \arg\max_v \sum_{k=1}^{K} \ln p_{\boldsymbol{y}} \left(\boldsymbol{x}_1, \boldsymbol{y}(k), \hat{\boldsymbol{\Sigma}}_1^{(\infty)}, v\right) \quad (14)$$

Under $\mathcal{H}_0$, we calculate $\hat{v}_0^{(j+1)}$ using $\boldsymbol{x} = \boldsymbol{0}$ and $\hat{\boldsymbol{\Sigma}}_0^{(\infty)}$ in (14).

The GLR test computed upon convergence of (12), (13) and (14) in (9) under $\mathcal{H}_0$ and $\mathcal{H}_1$, results in a complicated form which is impossible to statistically analyze. Therefore, we simplify it to the ratio of determinants of the covariance estimates under different hypotheses, (see (15)), which is also similar to the general form of GLR test presented in [11], to analyze its statistical characteristics (see Section IV). First we assume known texture components and compute the GLR test accordingly. Then using the data from the target-free neighboring cells as the secondary data, we run the inner and outer loops of the estimation algorithm to compute the conditional mean of the texture components in (11) given the secondary data. We replace the texture components with their corresponding conditional mean values reducing the GLR test to

$$\lambda = \frac{\left|T_2^{(\infty)}\right|}{\left|T_2^{(\infty)} - Q^{(\infty)} \left(S^{(\infty)}\right)^{-1} T_1^{(\infty)} \left(T_3^{(\infty)}\right)^{-1} \left(T_1^{(\infty)}\right)^{-1}\right|} \gtrless \eta \quad (15)$$

where $|\cdot|$ is the determinant operator, and $T_1^{(\infty)}$, $T_2^{(\infty)}$, $T_3^{(\infty)}$, $S^{(\infty)}$ and $Q^{(\infty)}$ are obtained in one step using (12) with (11) computed using the secondary data as just explained.

IV. Adaptive Design

In this section, we first demonstrate the asymptotical statistical characteristics of the detection test derived in Section III. Based on this result, we then construct a utility function for adaptive energy allocation to improve the detection performance. We determine the optimum transmitted energy by each transmitter according to this utility function.

We investigate the statistical properties of the test in (15), λ assuming that the texture components are known; that is, $w(k)$, $k = 1, \ldots, K$, are known. With this assumption the test is the complex version of Wilks' lambda, and under the null hypothesis ($\mathcal{H}_0$) it is shown to follow the probability density function of multiplication of complex beta random variables. However the exact statistical analysis of this test under alternative hypothesis ($\mathcal{H}_1$) is very difficult, except for some special cases; thus the distributions are mostly approximated [17]. Therefore, following our work in [18], we employ asymptotical approximations for the distributions of the tests, and we find, applying a similar approach used for real Gaussian random variables in [19], [20], that under $\mathcal{H}_0$, as $K \to \infty$, $K \ln \lambda$ has a complex chi-square distribution with NM degrees of freedom. For known texture components, the distribution under $\mathcal{H}_0$ does not depend on the speckle covariance; hence, in the limit it is a constant false-alarm rate (CFAR) test.

Under $\mathcal{H}_1$, as $K \to \infty$, $K \ln \lambda$ has a non-central complex chi-square distribution with NM degrees of freedom. That is, $K \ln \lambda \sim \mathbb{C}\chi^2_{NM}(\delta)$ [19] , [21]. The non-centrality parameter is $\delta = \mathrm{tr}\left(\boldsymbol{\Sigma}^{-1}(\boldsymbol{A}\boldsymbol{x}\boldsymbol{\phi})(\boldsymbol{A}\boldsymbol{x}\boldsymbol{\phi})^H\right)$

In practice the texture components are unknown and we replace them by their conditional mean values computed given the secondary data. Since the unknown parameters $\boldsymbol{\Sigma}$, and v of the secondary data belong to a canonical exponential family (since the complete-data likelihood function belongs to an exponential family and could be written in canonical form), their estimates are consistent and hence the conditional mean value in (11), computed given the secondary data, converges to the minimum mean square error estimate of the texture component in probability [15]. Then, in the mean, the detection performance of the detector with known texture provides an upper bound for the one with unknown texture. Optimizing the upper bound provides a way to optimize the detection performance. Therefore, we use the performance characteristics of the detector with known texture components computing a utility function for adaptive energy allocation to optimize the detection performance.

We observe that detection performance is optimized by maximizing the detection probability for a fixed value of probability of false alarm. It is shown in [21] that, under asymptotic approximation, the non-centrality parameter and probability of detection are positively proportional. Therefore we maximize the non-centrality parameter with respect to the energy parameters, β_m, $m = 1, \ldots, M$ (see (3) and (4) for the relation between the non-centrality parameter, and β's). We also incorporate an energy constraint in the maximization, $\sum_{m=1}^{M} |\beta_m|^2 = E$, such that the total transmitted energy is the same, independent of the system configuration and energy distribution. We define $\boldsymbol{\beta} = [\beta_1, \ldots, \beta_M]^T$, then the

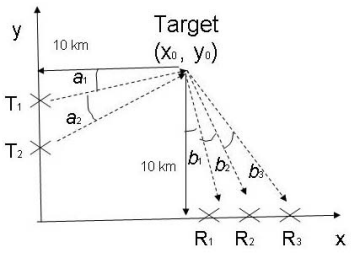

Fig. 1. MIMO antenna system with M transmitters and N receivers.

optimization problem reduces to

$$\hat{\boldsymbol{\beta}} = \underset{\boldsymbol{\beta}}{\operatorname{argmax}} \left[\operatorname{tr}(\boldsymbol{\Sigma}^{-1}(\boldsymbol{A}\boldsymbol{x}\boldsymbol{\phi})(\boldsymbol{A}\boldsymbol{x}\boldsymbol{\phi})^H) - \mu(\sum_{m=1}^{M} |\beta_m|^2 - E) \right], \tag{16}$$

where μ is the Lagrange multiplier. Without loss of generality, we assume $E = 1$, then after some algebraic manipulations using the structure of matrix $\boldsymbol{A}$ from (4), we show that this optimization problem further reduces to

$$\hat{\boldsymbol{\beta}} = \underset{\boldsymbol{\beta} \;\text{s.t}\; \boldsymbol{\beta}^T\boldsymbol{\beta}=1}{\operatorname{argmax}} \left[\boldsymbol{\beta}^T \boldsymbol{Q} \boldsymbol{\beta} \right], \tag{17}$$

where $\boldsymbol{Q}$ is computed using $\boldsymbol{\Sigma}$, $\boldsymbol{A}$ and $\boldsymbol{x}$. This equation has a unique solution such that $\hat{\boldsymbol{\beta}}$ is the eigenvector corresponding to the largest eigenvalue of the matrix $\boldsymbol{Q}$.

Note that $\boldsymbol{\Sigma}$, $\boldsymbol{x}$ are unknown in practice and we replace them with their estimates.

V. Numerical Examples

We present numerical examples using Monte Carlo (MC) simulations to illustrate our analytical results. We show the receiver operating characteristics and improvement in detection performance due to adaptive energy allocation for the MIMO system. The results are obtained from $2 * 10^4$ MC runs. We follow the scenario shown in Fig. 1. We assume that our system is composed of M transmitters and N receivers, where the antennas are widely separated. The transmitters are located on the y-axis, whereas the receivers are on the x-axis; the target is 10km from each of the axes; the antenna gains (G_{tx} and G_{rx}) are 30dB; the signal frequency (f_c) is 1GHz. The angle between the transmitted signals $a_1 = a_2 = ... = a_M = 10^\circ$ and similarly between the received signals $b_1 = ... = b_N = 10^\circ$. Hence R_m, $m = 1, \ldots, M$, and R_n, $n = 1, \ldots, N$, in (1) are calculated accordingly. In this scenario, all the transmitters and receivers see the target from different angles. Throughout the numerical examples, we choose $M = 2$ and $K = 40$ pulses for each transmitted signal.

We choose the spatial covariance of the speckle components in a block diagonal form ($\boldsymbol{\Sigma} = \operatorname{blkdiag}[\boldsymbol{\Sigma}_1, \ldots, \boldsymbol{\Sigma}_M]$) due to the assumption of low–cross-correlation signal transmission, see eqns. (2) and (3). $\boldsymbol{\Sigma}_m$, $m = 1, \ldots, M$, are positive definite $N \times N$ matrices with entries $\boldsymbol{\Sigma}_m[i,j] = \rho_s^{|i-j|}$, with $i, j = 1, \ldots, N$. This form of covariance ($\rho_s = 0.3$) for MIMO radar is used in [7] to account for the correlation between the received signals at different receivers due to the same transmitter. The target parameters $\boldsymbol{x}$ are chosen randomly for simulation purposes; that is, the entries are assigned as the realizations of a zero mean complex Gaussian random variable with unit variance. Later, $\boldsymbol{x}$ is scaled to meet the desired signal-to-clutter ratio (SCR) conditions. We define the SCR similar to [9] in (18). Moreover, the shape parameter of the texture component is chosen to be $v = 4$ (values between 3 and 9 are often good choices for heavy tail fitting [16]).

$$\mathrm{SCR} = \frac{1}{K} \frac{\sum_{k=1}^{K} (\boldsymbol{A}\boldsymbol{x}\phi(k))^H (\boldsymbol{A}\boldsymbol{x}\phi(k))}{\mathrm{E}\{u(k)\} \operatorname{tr}\boldsymbol{\Sigma}}. \tag{18}$$

We compare the receiver operating characteristics (ROC) of MIMO radar with conventional phased-array (Conv.) radar in Fig. 2(a). MIMO $M \times N$ and Conv. $M \times N$ stand for the MIMO and conventional radar systems, respectively, with M transmitters and N receivers. The model of Conv. radar is obtained from (1) using the fact that all the channel coefficients of the system (target RCS and distances of the radars to the target) are the same, since each transmitter and receiver pair sees the target from the same angle and distance. For fairness of comparison, the total transmitted energy, E, is kept the same for both Conv. and MIMO systems.

In Fig. 2(a), we assume for that spatial correlation $\rho_s = 0.3$, SCR=-10 dB, and the total energy is equally divided among the transmitters. In MIMO radar applications, the use of multiple orthogonal waveforms results in $10\log_{10}(M)$ dB loss in SCR [1, Chapter8]. Then, for fair comparison, we set SCR=-7 dB for Conv. system. As expected when the number of the receivers, N, increases, the performances of both MIMO and Conv. radar systems improve. However, MIMO radar always outperforms Conv. radar. The observed advantage of MIMO over Conv. radar stems from the diversity gain obtained by multiple looks at the target. That is, MIMO radar systems have the ability to exploit the spatial diversities, gaining sensitivity about the RCS variations of the target to enhance system performance.

In Fig. 2(b), we demonstrate the improvement in the detection performance due to the adaptive energy allocation. We compute the receiver operating characteristics for MIMO radar when the total energy (E) is equally divided among the transmitters (MIMO $M \times N$ on the figure) and subsequently when E is adaptively distributed among the transmitters using our algorithm (MIMO $M \times N$ Adap. on the figure). We assume SCR=-13dB (calculated for the equally distributed energy scenario) which is different than the value chosen for Fig. 2(a) to clearly demonstrate the effect of our adaptive algorithm. The adaptive method optimally allocates the total energy to transmitters depending on the target RCS values such that the signal-to-clutter ratio increases for the same total energy, E, and environment conditions. Increasing the SCR under the same target and environment conditions also increases the performance.

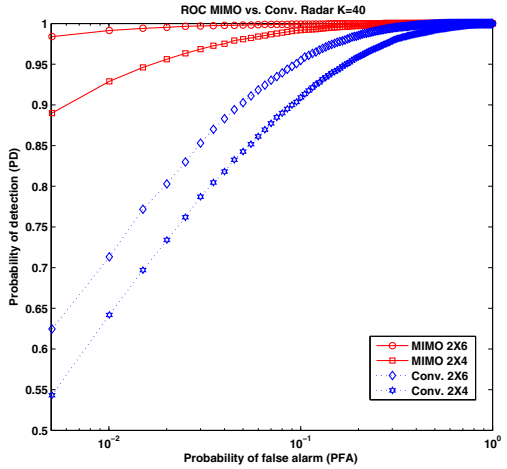

(a)

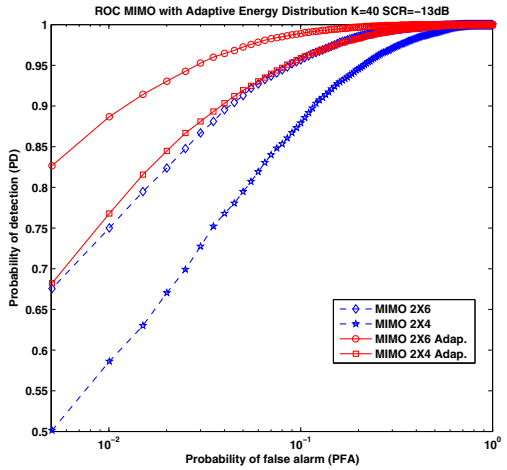

(b)

Fig. 2. (a) Receiver operating characteristics of MIMO and conventional phased-array radar (Conv.). (b) Receiver operating characteristics of MIMO radar with and without adaptive energy allocation.

VI. Concluding Remarks

We developed a statistical detector based on GLR for a MIMO radar system in compound-Gaussian clutter with inverse gamma distributed texture when the target and clutter parameters are unknown. First, we introduced measurement and statistical models within the GMANOVA framework and applied the PX-EM algorithm to estimate the unknown parameters. Using these parameters, we developed the statistical decision test detector. Moreover, we asymptotically approximated the statistical characteristics of this decision test and used it to propose an algorithm to adaptively distribute the total transmitted energy among the transmitters. We used Monte Carlo simulations and demonstrated the advantage of MIMO over conventional radar for target detection and the detection performance enhancement due to our adaptive energy distribution algorithm. Our future work will focus on robust MIMO detectors.

References

[1] J. Li and P. Stoica, *MIMO Radar Signal Processing*. Wiley-IEEE Press, Oct. 2008.

[2] E. Fishler, A. Haimovich, R. Blum, L. Cimini, D. Chizhik, and R. Valenzuela, "Spatial diversity in radars - models and detection performance," *IEEE Trans. Signal Process.*, vol. 54, no. 3, pp. 823–838, Mar. 2006.

[3] A. Sheikhi and A. Zamani, "Temporal coherent adaptive target detection for multi-input multi-output radars in clutter," *Radar Sonar and Navigation IET*, pp. 86–96, Apr. 2008.

[4] K. Ward, C. Baker, and S. Watts, "Maritime surveillance radar. I. Radar scattering from the ocean surface," in *IEE Proc. F*, vol. 137, Apr. 1990, pp. 51–62.

[5] F. Gini, A. Farina, and G. Foglia, "Effects of foliage on the formation of K-distributed SAR imagery," *Signal Processing*, vol. 75, pp. 161–171, Jun. 1999.

[6] M. Greco, F. Bordoni, and F. Gini, "X-band sea-clutter nonstationarity: Influence of long waves," *IEEE J. Ocean. Eng.*, vol. 29, no. 2, pp. 269–283, Apr. 2004.

[7] P. Sammartino, C. Baker, and H. Griffiths, "Adaptive MIMO radar system in clutter," *Radar Conference 2007 IEEE*, pp. 276–281, Apr. 2007.

[8] A. Balleri, A. Nehorai, and J. Wang, "Maximum likelihood estimation for compound-Gaussian clutter with inverse gamma texture," *IEEE Trans. Aerosp. Electron. Syst.*, vol. 43, no. 2, pp. 775–779, 2007.

[9] J. Wang, A. Dogandzic, and A. Nehorai, "Maximum likelihood estimation of compound-Gaussian clutter and target parameters," *IEEE Trans. Signal Process.*, vol. 54, no. 10, pp. 3884–3898, Oct. 2006.

[10] M. Akcakaya, M. Hurtado, and A. Nehorai, "MIMO radar detection of targets in compound-Gaussian clutter,," in *Proc. 42nd Asilomar Conf. Signals, Syst. Comput.*, Pacific Groove, CA, USA, Oct. 2008 (invited).

[11] A. Dogandzic and A. Nehorai, "Generalized multivariate analysis of variance: A unified framework for signal processing in correlated noise," *IEEE Signal Process. Mag.*, vol. 20, pp. 39–54, Sep. 2003.

[12] C. Liu, D. Rubin, and Y. Wu, "Parameter expansion to accelerate EM: The PX-EM algorithm," *Biometrika*, vol. 85, pp. 755–770, Dec. 1998.

[13] S. M. Kay, *Fundamentals of Statistical Signal Processing: Detection Theory*. Upper Saddle River, NJ: Prentice Hall PTR, 1998.

[14] Y. Abramovich and G. Frazer, "Bounds on the volume and height distributions for the MIMO radar ambiguity function," *IEEE Signal Processing Letters*, vol. 15, pp. 505–508, 2008.

[15] P. Bickel and K. Doksum, *Mathematical Statistics: Basic Ideas and Selected Topics*, 2nd ed. Upper Saddle River, NJ: Prentice Hall, 2000.

[16] K. Lange, R. Little, and J. Taylor, "Robust statistical modeling using the t distribution," *Journal of the American Statistical Association*, vol. 84, no. 408, pp. 881–896, 1989.

[17] E. J. Kelly and K. M. Forsythe, "Adaptive detection and parameter estimation for multidimensional signal models," Lincoln Laboratory, MIT, Lexington, MA, Tech. Rep. 848, Apr. 1989.

[18] S. Sen and A. Nehorai, "Target detection in clutter by an adaptive OFDM radar," *IEEE Signal Processing Letters*, to be published.

[19] T. W. Anderson, *An Introduction to Multivariate Statistical Analysis*, 2nd ed. Wiley, Sep. 2003.

[20] E. F. Vonesh and V. Chinchilli, *Linear and Nonlinear Models for the Analysis of Repeated Measurements*, 1st ed. Dekker, 1996.

[21] Y. Fujikoshi, "Asymptotic expansions of the non-null distributions of three statistics in GMANOVA," *Annals of the Institute of Statistical Mathematics*, vol. 26, no. 1, pp. 289–297, Dec. 1974.